Locomotion Selectively Amplifies Sensitizing Neurons in Primary Visual Cortex

Kosiachkin Ye.[1,*], Hinojosa A.J.[1,*], Dominiak S.E.[1], Evans B.D.[2], Lagnado L.[1]

1. Sussex Neuroscience, School of Life Sciences, University of Sussex, Brighton BN1 9QG, UK
2. AI Research Group, School of Engineering and Informatics, University of Sussex, Brighton BN1 9QG, UK
* These authors contributed equally. Correspondence to L. Lagnado

Abstract

Sensory processing in the cortex is shaped both by adaptation to external stimuli and by changes in internal state but it is not known how these processes interact, in large part because neuromodulatory changes in synaptic strength are difficult to quantify in behaving animals. Here we combine two-photon calcium imaging, optogenetics and circuit modelling to investigate how locomotion adjusts adaptation in layer 2/3 of mouse primary visual cortex (V1). We show that this change in state preferentially increases gain in PCs that sensitize during a high-contrast visual stimulus, while having weaker effects on PCs that depress. A population model constrained by a number of optogenetic manipulations accounts for the differential modulation of PCs during locomotion on the basis of i) variations in the connections that individual PCs receive from PV and SST interneurons, ii) a broad weakening of PC and PV synapses to all local targets, and iii) enhanced inhibition from SST synapses targetting depressing PCs. These results provide a quantitative and integrated understanding of how state-dependent modulation of cortical circuits can selectively bias cortical computation toward different adaptive regimes. The apparently paradoxical combination of increased PC gain but decreased synaptic strength suggests a state-dependent gating mechanism that boosts signals leaving V1 for higher visual areas while simultaneously preventing disruption of the excitatory-inhibitory balance required for stable local computation.

Introduction

Sensory processing in the cortex is adjusted both by adaptation to the external environment and changes in the internal physiology of the animal that generate behavioural states such as attention, arousal and satiety[1-5]. The mechanisms by which external and internal variables interact within the cortical circuitry are not understood. Here we investigate this question by analyzing how the change in state associated with locomotor activity impacts adaptation in primary visual cortex (V1) of mice[6].

The dynamics of neurons in V1 reflect adaptation on multiple time-scales. In pyramidal cells (PCs), the initial excitatory response to an increase in contrast is followed by a fast (subsecond) decrease in gain reflecting depression in feedforward inputs from the LGN[7,8]. This is immediately followed by a slower phase of adaptation that varies dramatically across the PC population: while some PCs depress in response to a high-contrast stimulus others simultaneously *sensitize*[9]. PCs within layer 2/3 are not, therefore, a homogenous population: to understand gain control we must take into account variations in local inhibitory circuits in which they are embedded.

The onset of locomotion signals changes in internal state associated with attention or arousal, acting in less than a second to amplify visual responses in PCs[3,10-12]. A major driver of this increase in gain are cholinergic fibers arriving from the basal forebrain[2,13-15]. A minority of fibers make direct synaptic connections that excite interneurons expressing vasoactive intestinal peptide (VIP)[16], leading to amplification of PC responses through a VIP->SST->PC disinhibitory pathway. The majority of the cholinergic input, however, innervates V1 diffusely to modulate circuit function through extra-synaptic (muscarinic) receptors[2,13,16]. In vitro experiments, have shown that M1 and M3 receptors on soma and dendrites of PCs can increase excitability while M2 receptors on axonal compartments reduce synaptic release probability[16-18]. Accounting for state-dependent changes in cortical processing therefore requires an integrated understanding of changes in both electrical activity and the strength of synaptic connections[12]. The difficulty, however, is that modulations of synaptic strengths are very hard to quantify in awake and behaving animals: recording from connected neuron pairs remains technically challenging and is limited to anaesthetized animals in which inhibitory microcircuits are severely compromised [19-21]. Current knowledge about synaptic modulation in cortical circuits is derived from *ex vivo* studies or inferred from indirect *in vivo* observations and modelling [12,22].

To understand how locomotion and adaptation interact in V1 of mice we used calcium imaging to record visual responses in PCs and the three major classes of interneuron (VIP, SST and PV), optogenetics to identify key interactions and a data-driven circuit model to estimate changes in synaptic weights. We demonstrate that long-range inputs to VIPs that increase visual gain in the locomoting state also govern the time-course of adaptation over the behavioural time-scales of seconds. These inputs do not act uniformly across the PC population but preferentially

increases the gain of sensitizing neurons. Contrary to the prevailing model of gain control through the VIP->SST->PC pathway we find that visual responses in SSTs are not inhibited by locomotion but instead weakly enhanced. These observations can be reconciled by also taking into account neuromodulatory changes in synaptic strength, and our results predict a decrease in the strength of connections from PCs to all their targets and an increase in the strength of inhibitory connections made by SSTs. Locomotion preferentially increases the gain of PCs that undergo the sensitizing form of adaptation because these are at least seven times more strongly connected to SSTs compared to PVs. These results provide an integrated view of the circuit mechanisms which cause locomotion-dependent changes in gain to interact with adaptation to adjust visual processing in V1.

Results

Differential effects of locomotion on the fast and slow phases of adaptation

To understand how changes in brain state interact with adaptation in V1 we used two-photon calcium imaging to measure the activity of excitatory and inhibitory neurons in layer 2/3 during periods of rest and locomotion (Fig 1A, see Methods). The GCaMP6f signal in PCs responding to a high contrast stimulus (20º drifting grating at 1 Hz, 10 s duration) are shown in Fig. 1B. Locomotion increased the response averaged across all PCs by a factor of 2.2 ± 0.9. The dynamics of individual neurons, however, varied widely: some PCs responded with high initial gain and then depressed, while others responded with low initial gain and then sensitized. This heterogeneity is illustrated by the raster plot in Fig. 1B which shows 522 neurons ordered by the time of peak activity: depression (early peak) and sensitization (late peak) were similarly represented in the two behavioural states (Fig 1B, top).

The increase in gain during locomotion was manifested in two ways; a 6-fold increase in the number of PCs generating a significant response (Table 1) and an increase in the average amplitude of these responses measured as the integral during the 10 s stimulus (Fig. 1B). To investigate how these changes in gain affected PCs undergoing different forms of adaptation we split the population into three groups of equal size based on the distribution of a metric called the adaptive index (AI; Methods). These groups were sensitizing (AI less than zero), intermediate and depressing (AI more than zero; Fig. 1C). The AI averaged across the whole PC population was similar during locomotion (-0.006 ± 0.3; mean ± sem) and rest (0.001 ± 0.9; Fig. 1C) but the amplitude of the visual response increased by a factor of 4.5 ± 0.7 in sensitizing PCs, 2.5 ± 0.3 in intermediate group and 2.2 ± 0.2 in depressors. Locomotion therefore increased the gain of sensitizing PCs about twice as strongly as depressors (Fig. 1D-G).

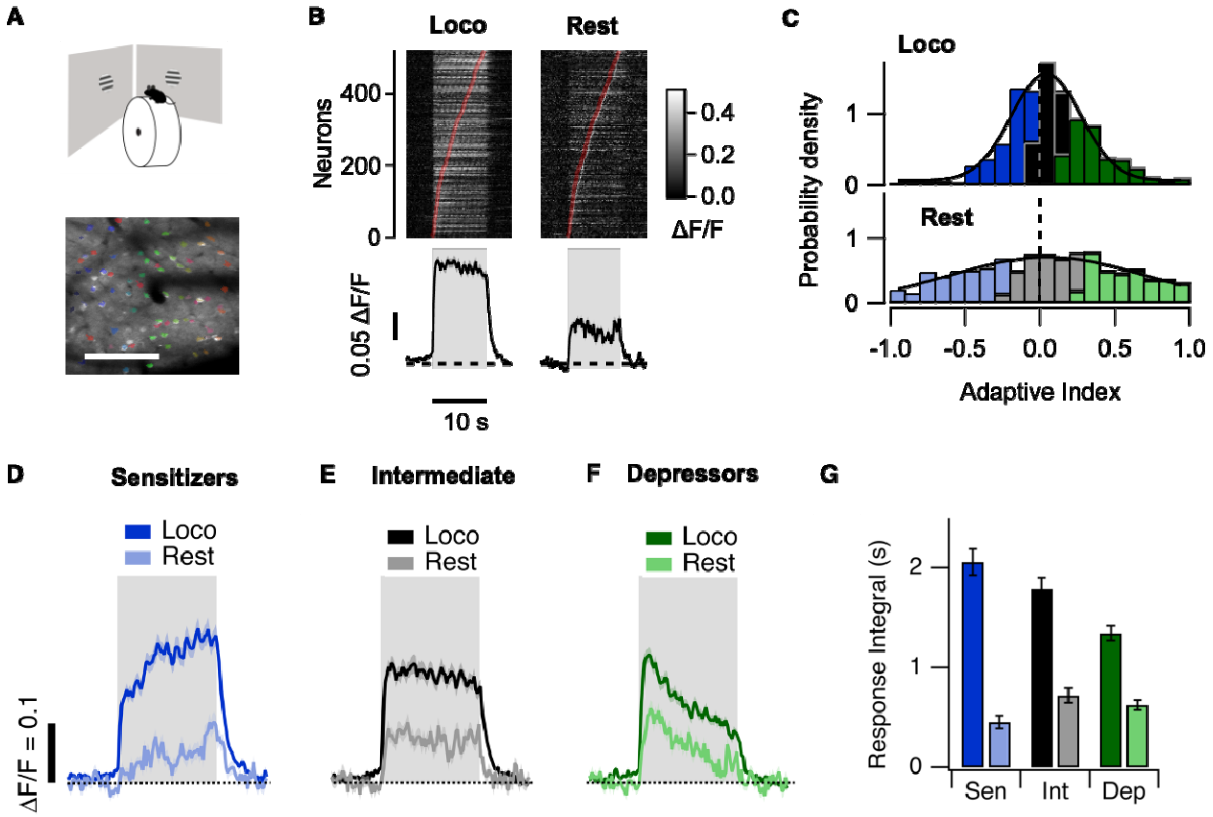

Figure 1. Slow adaptation in pyramidal cells during rest and locomotion.

A. Mice running on a treadmill were shown a visual stimulus (drifting grating, 20º in size) for 10 seconds (top). Example field of view (FOV) showing PCs in V1 expressing GCaMP6f (grey) and corresponding regions-of-interest (ROIs) for individual neurons (rainbow). Scale bar represents 200 µm. **B.** Top: raster plots showing average calcium responses from individual PCs that were responsive to the stimulus during locomotion and rest (n = 522 neurons, from 9 mice). Responses are averaged over 10 stimulus trials then sorted by time of maximum amplitude. Bottom: average calcium response of all PCs to the visual stimulus during locomotion (left) and rest (right). **C.** Distributions of adaptive indexes (AIs) in the PC population during locomotion (top) and rest (bottom) in sensitizers (blue), intermediate cells (grey) and depressors (green). Both distributions can be described by gaussians with similar x_0 and different width (rest, 0.001±0.9; Loco, -0.006±0.3). **D, E, F.** Splitting the distribution of PCs according to their AI reveals that the tertile with lower AI showed slow sensitization, the tertile with intermediate values showed little adaptation, and the tertile with higher AI showed slow depression. **G.** Differences in gain of sensitizers (blue), intermediate cells (grey) and depressors (green) measured as the integral during the stimulus show that locomotion caused a stronger gain increase in sensitizers than in depressors ($p < 0.001$, Linear Mixed Model).

	Rest (N, per FOV)	**Locomotion** (N, per FOV)	**Relative Change**
PC	4.4 ± 1.1	27.8 ± 2.0***	6.3 ± 1.7
SST	5.1 ± 1.0	6.2 ± 0.7	1.2 ± 0.3
PV	10.1 ± 2.2	18.4 ± 1.6***	1.8 ± 0.4
VIP	11.7 ± 6.2	34.9 ± 3.2*	3.0 ± 1.6

Table 1. Locomotion-related changes in the number of neurons responding to the visual stimulus. The number of cells of each type generating a significant response to the stimulus at rest per field of view (FOV) of 0.2 mm^2; mean ± sem; n = 11, 8, 16, 6 FOVs for PCs, SSTs, PVs and VIPs, respectively) and during locomotion (n = 55, 23, 35, 22). Locomotion had no significant effect on the number of responsive SSTs. The increase in the number of responsive PCs and PVs was significant at $p < 0.001$ and at $p < 0.05$ for VIPs. The relative change is the ratio of the number of responsive neurons during locomotion compared to rest.

The immediate spiking response to a high-contrast stimulus is dominated by depressing adaptation[7,8] but the raw signal from calcium reporter proteins such as GCaMP does not easily distinguish this phase because of the gradual accumulation of calcium in the neuron. Several algorithms for estimating spike rates from calcium signals are now in use[23-25] and we applied MLspike because it is based on a biological model of GCaMP activation and calcium dynamics that has been shown to perform better than others[26 26]. The first component of the spiking response was followed by fast depressing adaptation, as expected from electrophysiology[7,8,27] (red arrows In Fig. 2A-B). During locomotion, the initial peak amplitude was not significantly different in PCs that depressed (1.15 ± 0.08 Hz) or sensitized (1.11 ± 0.08 Hz), indicating similar actions of the feedforward input across the PC population (Fig. 2C).

Comparing activity at rest and while running revealed a powerful effect on both first and second phases of the response but this varied across the PC population. In the sensitizing tertile the initial peak driven by feedforward input underwent a relative change of 2.1 ± 0.7, calculated as (response locomoting – response at rest)/response at rest) and the response integrated over the whole stimulus a relative change of 4.7 ± 1 (Fig. 2D). But in the depressing tertile, locomotion did not significantly change the initial fast response while the integrated response only increased by a factor of 1.4 ± 0.3 (Fig. 2E). Changes in internal state associated with locomotion do not, therefore, act uniformly across the PC population but preferentially increase the gain of neurons that undergo the sensitizing form of adaptation.

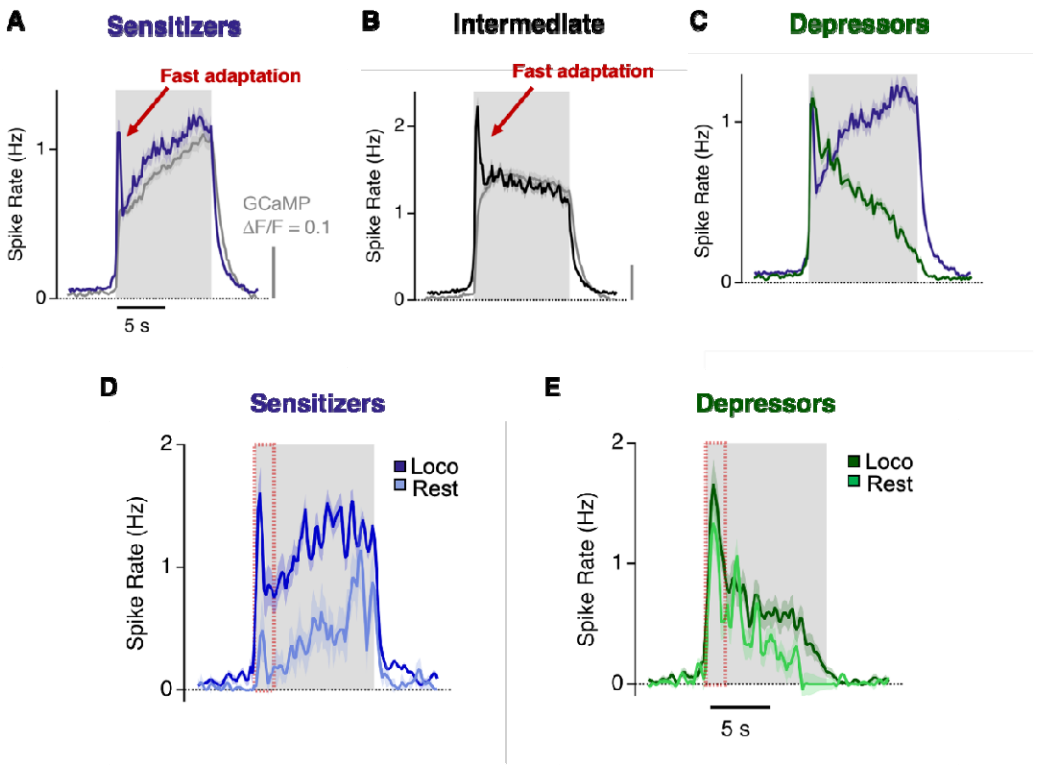

Figure 2. Differential effects of locomotion on fast and slow components of adaptation. **A.** Estimated spike rate averaged across all sensitizing PCs measured during locomotion (n = 479 neurons from 14 mice). The GCaMP signal averaged across the same set of neurons is shown in grey. The fast depressing component of adaptation is highlighted by the red arrow. **B.** As A, but for the second (pre-dominantly non-adapting) tertile of PCs. **C.** Comparison of average spiking response in the sensitizing and depressing tertiles. Note the almost identical initial amplitude. **D.** Comparison of average spiking response at rest and during locomotion in the third (sensitizing) tertile of PCs in which paired measurements were made. Paired measurements were made in 158 neurons in 9 mice. The relative change in the response during locomotion was 4.7 ± 1. **E.** Comparison of average spiking response at rest and during locomotion in the depressing tertile of PCs. The relative change in the response during locomotion was 1.4 ± 0.3 which was significantly smaller than sensitizing tertile ($p < 0.001$).

A data-driven model of contrast adaptation and the effects of locomotion

To understand how locomotion preferentially modulates PCs undergoing the sensitizing mode of adaptation we constructed a population model of signal flow based on neuronal input-output functions expressed as firing rates[28-30] (see Methods). The aim was *not* to provide a comprehensive description of all the processes that might operate on the time-scales of the visual responses, such as different modes of synaptic plasticity: our aim was to understand key features that could explain the link between adaptative changes and the locomoting state shown in Fig. 2D and E. The model took into account three aspects of circuits in layer 2/3: *i)* the measured response dynamics of PCs (Fig. 2) and the three major types of interneurons (Fig. 3); *ii)* the dynamics of signals that arrive from other brain regions (Fig. 4A), and *iii)* the known connectivity

patterns of neurons within this layer (Fig. 4B). Code and example data sets at https://github.com/lagnadoLab/CortexModel.

i) The dynamics of neurons in layer 2/3

A key determinant of the magnitude and direction of slow adaptive changes in a PC is the local inhibitory microcircuit in which it is embedded: PCs in which direct SST inputs dominate over PV inputs tend to sensitize while those in which PV inputs dominate depress[9]. We therefore also measured the effects of locomotion on gain and adaptation of the three major types of interneurons (Fig. 3). VIPs underwent the strongest modulation: the density of responsive neurons increased by a factor of 3 (Table 1), and the amplitude of these responses increased by factor of 5.1 ± 1.0 (Fig. 3A). Simultaneously, locomotion caused the ratio of sensitizing (AI <0) to depressing (AI > 0) VIPs to increase from 1.3 at rest to 9 (Fig. 3D). PVs were more weakly modulated, with a gain factor of 1.7 ± 0.2 while the ratio of sensitizers to depressors also increased from 1.8 to 6.1 (Fig. 3B and E). In contrast, locomotion did not significantly alter the number of responsive SST neurons or the amplitude of their responses (gain factor of 1.2 ± 0.2; p = 0.28; Fig. 3C and F). This observation was surprising given that VIPs powerfully inhibit SSTs and locomotion activates a VIP->SST->PC disinhibitory pathway proposed to be the major mechanism of gain control[11,31,32]. A major aim of the model, therefore, was to take a more integrated view of gain control that considered multiple interacting pathways within layer 2/3.

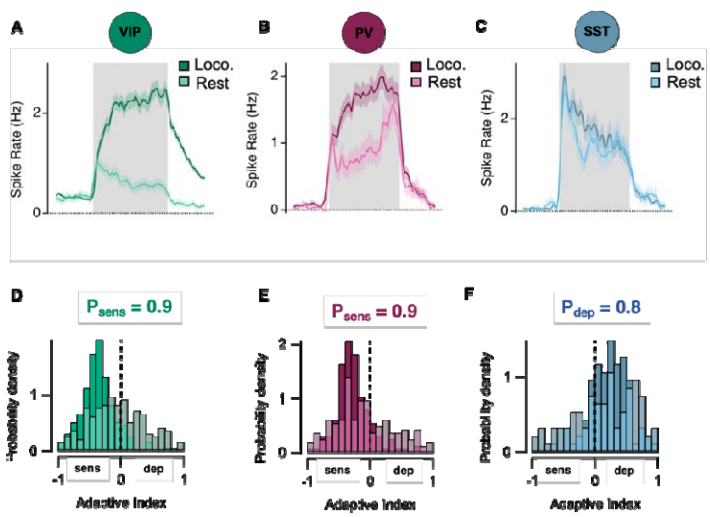

Figure 3. Differential effects of locomotion on the gain of interneurons.

A. Average response of VIPs to the visual stimulus during locomotion and rest. The gain during locomotion increased by factor of 5.1 ± 1.0, measured from the integral of the responses. **B.** Average response of PVs to the visual stimulus during locomotion and rest. The gain during locomotion increased by factor of 1.7 ± 0.2. **C.** Average response of SSTs to the visual stimulus during locomotion. SSTs showed a much smaller, nonsignificant, gain change 1.2 ± 0.2, p = 0.28. **D.** Distribution of adaptive indices in VIP interneurons (n = 122 neurons in 2 mice). Note that AI was measured from GCaMP signals, as for PCs in Fig. 1. VIPs were predominantly sensitizing. P_{sens} = 0.56 at rest and 0.90 during locomotion. **E.** Distribution of adaptive indices in PVs (n = 97 neurons in 3 mice). PVs were predominantly sensitizing.

P_{sens} = 0.64 at rest and 0.86 during locomotion. **F.** Distribution of adaptive indices in SSTs (n = 82 neurons in 4 mice). SSTs were predominantly depressing at rest and during locomotion. P_{sens} = 0.37 at rest and 0.21 during locomotion.

The distribution of response dynamics in interneurons was more homogenous than PCs. In PCs, the probabilities of a neuron being sensitizing (AI <0) or depressing (AI > 0) were both ~0.5 (Fig. 1C), but during locomotion sensitization dominated in VIPs and PVs (P_{sens} = 0.9) while depression dominated in SSTs (P_{dep} = 0.8; Fig. 3D-F). We therefore used a population mean field model in which a single response dynamic, measured as the average shown in Fig. 3A-C, describes each type of interneuron. Mean field models have been widely used to describe the average behaviour of large populations of interacting neurons without simulating each neuron individually[28,33,34]. The network was represented by a system of four first order ordinary differential equations[28]:

$$\tau_i \frac{dr_i}{dt} = -r_i + f(\sum_j w_{ji} r_j + w_{in} In + b_i) \qquad (1)$$

where i, j are iterating through the four neuronal populations (PC, VIP, PV and SST), j is a presynaptic population and i postsynaptic, r is a firing rate and τ_i is the time-constant for that population. $f(x)$ is a neuronal input-output function and here we used a rectified power low[30]. The connection weight between populations *j* and *i*, w_{ji}, is simply the product of the total number of synaptic connections, C_{ji}, and the average strength of an individual synapse, s_{ji}:

$$w_{ji} = C_{ji} s_{ji} \qquad (2)$$

The total synaptic input that neuron i receives from j, I_{ji}, is proportional to the activity of j:

$$I_{ji} = w_{ji} r_j \qquad (3)$$

To compare the model to experiments it was important to consider that not all presynaptic neurons are activated by the stimulus and, even if they are, they will not all activate the postsynaptic population because the connection probability, p_{ji}, is usually less than one. If, for instance, electrodes are placed on a PC and a nearby PV interneuron the probability of them being connected is only ~0.37 at distances less than ~150 μm while the average probability of an SST interneuron is even lower at ~0.27[35-37]. These factors can be taken into account by expanding relation 2 as

$$w_{ji} = N_j p_{ji} s_{ji} \qquad (4)$$

where N_j is the number of *responsive* presynaptic cells, defined as described in Methods. Below we compare measured changes in N_j caused by locomotion (Table 1) to changes in w_{ji} estimated by fitting the model, allowing us to estimate changes in the strength of individual synapses based on the reasonable assumption that connection probabilities are constant on the time-scale of minutes.

ii) The dynamics of signals entering layer 2/3.

Excitatory signals entering layer 2/3 are of three main types[38,39]: feedforward (FF) drive originating from the lateral geniculate nucleus (LGN) and transmitted via layer 4, feedback from higher order cortices (FB)[40,41] and modulatory inputs (SM), such as cholinergic signals from the basal nuclei[11]. Electrophysiology has shown that FF inputs to layer 2/3 are dominated by fast depressing adaptation occurring within a few hundred milliseconds and the fast phase of adaptation in PCs fell within this range[7,8]. (Fig. 2A-B). Calcium imaging *in vivo* has shown that drifting gratings lasting seconds can also generate a slower sensitizing component in FF inputs that enter layer 2/3 from layer 4[22,42]. The FF input was therefore modelled with both these components, as shown in Fig. 4A.

The second type of input to V1 is feedback from higher visual areas[43-45] and SST interneurons are a major target for these[44,46,47]. We have limited understanding of the dynamics of the FB signal over the time-scale of our stimulus, so, for simplicity, it was modelled as a step beginning at a delay of 380 ms after stimulus onset (Fig. 4A).

The third type of inputs to layer 2/3 are visually-activated signals that are strongly sensitizing in the locomoting state and drive slow modulation. This input was based on the response of VIPs during locomotion, for three reasons. First, cholinergic inputs from the basal forebrain are known to powerfully activate VIPs during locomotion[11,48]. Second, we could reliably measure the dynamics of this input to layer 2/3 because the visual stimulus only weakly activated VIPs at rest but much more strongly during locomotion (Fig. 3A). Third, and crucially, optogenetic experiments confirmed that activity in VIPs drove adaptation in downstream SST neurons (Fig. 4C-D). To carry out this test we had to express the inhibitory photoprotein ArchT in VIPs and GCaMP6f in SSTs. Expressing different proteins in two interneuron populations was achieved by crossing a recombinant mouse line expressing Cre (VIP-Cre) with a Flippase expressing line (SST-Flp), then injecting two viral vectors that were Cre and Flippase dependent respectively (see Methods). Suppressing activity in VIPs almost completely abolished the slow component of adaptation in SSTs (Fig. 4D), to which they are known to connect strongly[11,31,32]. Visually-driven inputs to VIPs include local recurrent excitation[27] and inputs from higher visual areas[41], and their combined dynamics were modelled on the VIP response (Fig. 4E).

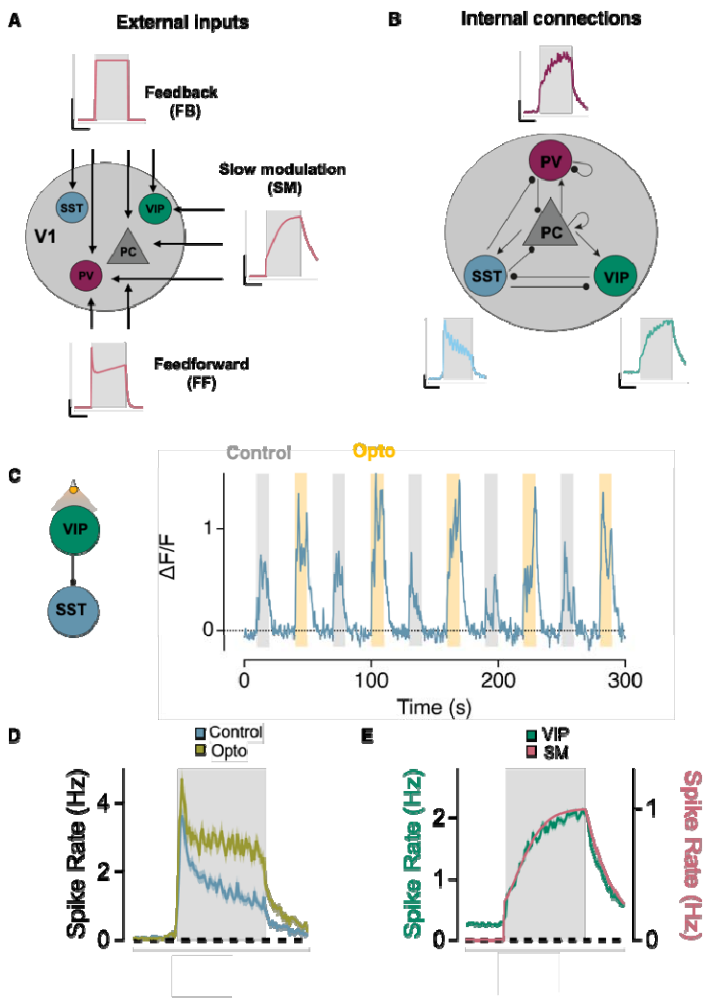

Figure 4. A model of signal flow in layer 2/3.

A. Schematic showing the targets of three external inputs. Feedforward excitation targets PVs and PCs; feedback input targets all populations [49,50] and the slower modulatory input enters through VIPs as well as directly activating PCs and PVs[51]. **B.** Schematic showing the main excitatory (arrow tip) and inhibitory (round tip) connections between cell types within L2/3 of V1. PCs form excitatory connections with all other neuron types including themselves. PVs mainly target PCs and other PVs while SSTs inhibit all other cell types but avoid inhibiting each other. VIPs almost exclusively inhibit SST interneurons. (Vertical bar: 0.05 ΔF/F, horizontal bar: 5 s). **C.** Left: schematic showing the experimental paradigm to test if VIPs were a target for a slow modulatory signal driving adaptation in layer 2/3: VIPs were silenced optogenetically while simultaneously recording activity in SSTs. Right: example response of an SST neuron during stimulus presentation alone and stimulus paired with optogenetic silencing of VIPs. **D.** Average response of SSTs with and without optogenetic silencing of VIPs (n = 83, from 4 mice). Silencing VIPs almost completely blocked slow adaptation. **E.** The slow modulatory input to the model (SM) was based on the average response of the VIP population during locomotion and consists of a step and sigmoid function with a time-constant = 1.71 s.

Notably, the dynamics of sensitization in VIPs were also similar to sensitization in PCs suggesting that this input dominated the dynamics of slow adaptation throughout the network (Supplementary Figure 1).

iii) Connectivity within layer 2/3

Cortical connections have been probed using a number of approaches, including viral tracing[52], electrophysiology[31,35,37] and optogenetics[36], and we only considered connections that have been consistently observed in layer 2/3 and are strong enough to significantly influence the circuit (Fig. 4B). Not all neuron types connect; SST interneurons, for example, do not interact with each other while the very small number of connections from VIPs to PCs were neglected because these are not strong enough to significantly influence the circuit[31,36].

Fine-tuning the model using optogenetics

The model was fit to average populational responses of PCs and interneurons by adjusting the weights w_{ji} of external and internal connections in layer 2/3 (see Methods for approach to fitting). In some cases, different sets of weights were capable of fitting the four neuronal populations similarly well. The model was therefore constrained further using additional datasets consisting of average PC responses measured during a series of optogenetic perturbations (Fig. 5). First, we expressed the excitatory photoprotein ChrimsonR in SSTs and GCaMP6f in PCs by using a Cre-dependent viral vector in SST-Cre mouse line and GCaMP6f in PCs under the CaMKII promoter. The intensity of the photo-activating light was adjusted to increase the activity of SST interneurons by an average factor of ~1.4 in locomoting animals, as estimated in a separate series of experiments[9]. Fig. 5A (top) shows how the average PC response was reduced compared to interleaved control trials; scaling the average SST activity within the model by a factor of 1.4 while leaving all other parameters constant provided an accurate description of the change in average

Reducing the activity of SSTs by an average factor of about ~2 using ArchT had the opposite effect - amplification of the average PC response - and this action was also quantitatively captured by the model (Fig. 5A, bottom). Similar manipulations of activity were carried out in PV interneurons (Fig. 5B) and again the model could describe changes in PC activity, further narrowing the set of weights describing activity in layer 2/3. These results demonstrate that the model incorporates enough features to accurately account for the visual responses of all the major neuronal classes across a range of conditions.

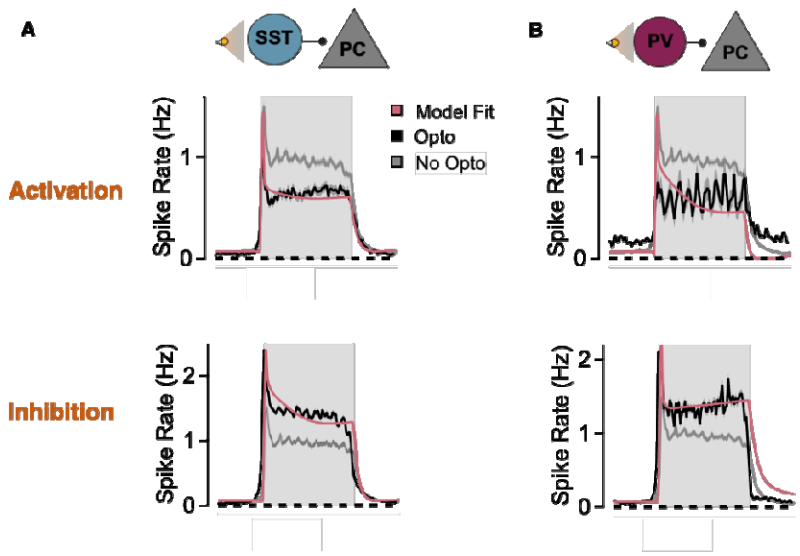

Fig. 5. Fine-tuning the model using optogenetics.

A. Top: Average PC response with and without optogenetic activation of SSTs. Separate experiments indicated that this intensity of photoactivating light increased SST activity by a factor of ~1.4[9]. The red trace shows the model prediction when SST activity within the model was increased by the same factor. Activation of SSTs decreased PC gain and increased sensitization (top, RMSE = 0.05). Bottom: Average PC response with and without optogenetic inhibition of SSTs. Separate experiments indicated that this intensity of photoactivating light decreased SST activity by a factor of ~2[9]. The red trace shows the model prediction when SST activity within the model was decreased by the same factor. Silencing of SSTs resulted in an increase in gain and a shift to more depressing dynamics (bottom, RMSE = 0.13). **B.** Same as in C but when PVs were optogenetically activated (top, by a factor of ~1.3) or silenced (bottom, by a factor ~1.6) during stimulus presentations. Activation of PVs decreased the gain of PCs (top, RMSE = 0.15). Silencing of PVs resulted in an increase in gain and shift to more sensitizing dynamics (bottom, RMSE = 0.11). Note that RMSEs in this case were calculated for 10 s timeframe, when stimulus was presented.

Locomotion increases PC gain but weakens their local synaptic output

First, we investigated the action of locomotion averaged across the whole PC population (Fig. 6) and then explored why the subsets of PCs that sensitize are modulated more strongly than those that depress (Fig. 7).

The fits of the model to the average visual responses in the four cell types closely followed both the fast and slow phases of adaptation at rest and during locomotion (Fig. 6A-D). The total connection weights at rest are shown in the heatmaps in Fig. 6E and the relative changes are summarized in Fig. 6F, calculated as

$$[w_{ij(loco)} - w_{ij(rest)}] \,/\, w_{ij(rest)} \qquad (5)$$

Where free parameters predicted by the model could be compared with published experiment, there were several points of agreement. For instance, variations in the strength of direct

connections to PCs were quantitatively similar to those measured using electrophysiology[35,36]. The model also predicted the locomotion-dependent amplification of the slowly modulated input to both VIPs[11] and PCs[51] and stronger feedforward drive to PCs[53,54].

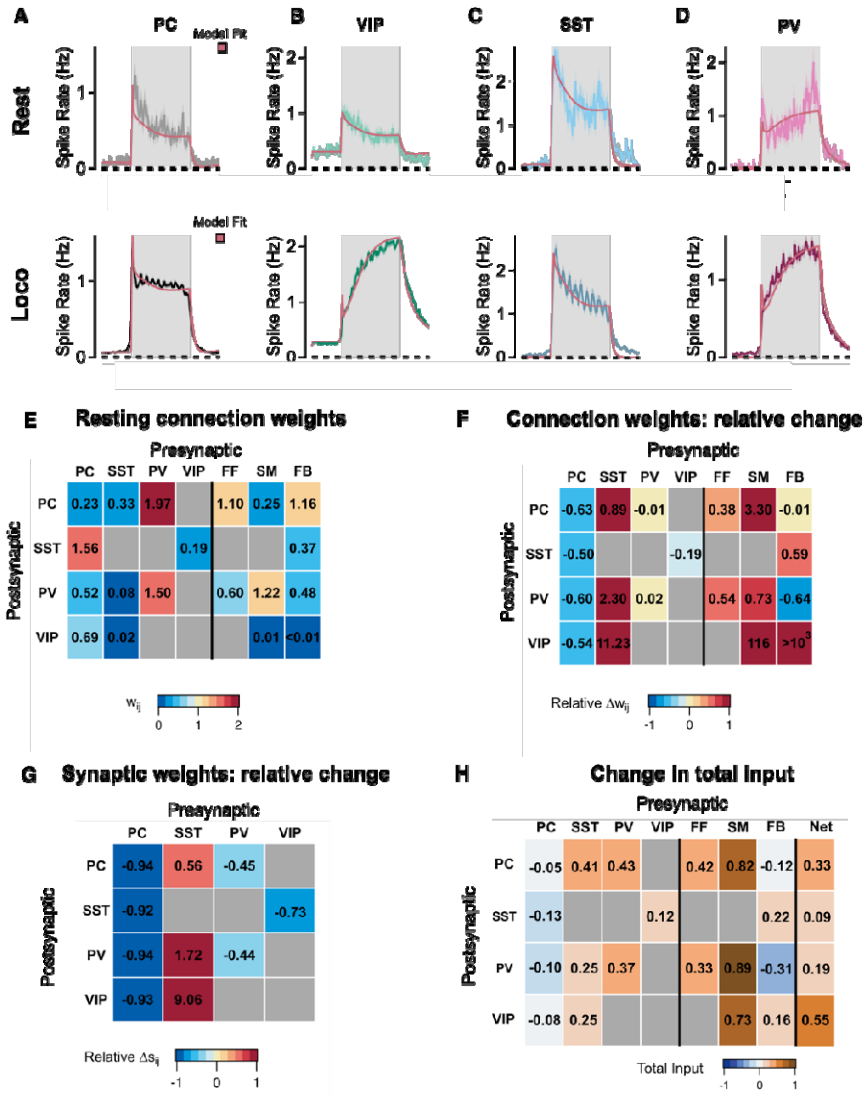

Figure 6. Locomotion modulates both electrical activity and the strength of synaptic connections.
A-D. Top: Average firing rates of PCs (A, black), VIPs (B, green), SSTs (C, blue) and PVs (D, dark red) during stimulus presentation at rest and their corresponding fits calculated by the model (light red, RMSE = 0.18). Note that these traces show the average activity of *responsive* neurons in each population. Bottom: average activity during locomotion in the same neurons (RMSE = 0.11). **E.** Resting connection weights estimated by fitting the model to the activity of responsive neurons (Equation 2). **F.** The relative change in connection weights caused by locomotion (Equation 5). Note that all SST outputs increase in weight while PC outputs decrease. **G.** Relative change in synaptic weights based on estimated changes in connection weights **(F)** and measured changes in number of responsive cells (Table 1; equation 5). **H.** The change in the total synaptic input activated by the stimulus, calculated from the average activity

(Figs. 1 and 3) and the change in connection weight in F (equation 3). The last column is the net change taking into account the polarity of the synapse.

Behavioural modulation of connection weights *within* layer 2/3 have been very hard to quantify experimentally, making it unclear how far changes in internal state adjust cortical processing through changes in neuronal activity as opposed to modulation of synaptic strength[14,16]. The model indicates that locomotion increases the gain of PCs through a broad combination of circuit effects but of particular importance is an approximate halving in the strength of inhibitory synapses made by PVs (Fig. 6G). This can be readily understood in terms of cholinergic modulation through M2 and M4 receptors that reduces release probability in PVs in visual[55], somatosensory[56] and auditory cortex[57].

Strikingly, the model also predicts a 50-60% *decrease* in the total weight of connections from PCs to all types of interneurons following locomotion. Taking into account the 5-fold *increase* in the number of responsive PCs during locomotion (Table 1 and equation 4) this leads to an estimated 90% decrease in synaptic strength across all PC targets (Fig. 6G). Experiments *in vitro* again suggest a mechanism – activation of M2 receptors on presynaptic compartments reducing release probability[16-18]: The insight here is that the large increase in PC and PV activity during locomotion is associated with a wide-spread decrease in the strength of their *local* synapses. This might represent a mechanism that allows large changes in the gain of signals *leaving* V1 for higher visual areas but without overexcitation of PC targets *within* the local circuit (see Discussion).

In contrast, the effects of locomotion were accounted for by an *increase* in the average weight of SST connections to all their targets (Fig. 6F) consistent with the observation that cholinergic projections facilitate SSTs through both nicotinic and muscarinic receptors in[31,58,59]. The number of responsive SSTs neurons increased by only 22% (Table 1) indicating that the major cause was a strengthening of SST synapses (Fig. 6G). Experiments *in vitro* have shown that ACh strongly enhances SST→PC inhibition via M1 receptor-mediated potentiation of $GABA_A$ currents on PCs[58,59].

Another way to summarize the effects of locomotion is to consider the change in the *total* synaptic input as PCs respond to the visual stimulus, which is the change in the weight of a connection multiplied by the activity of the presynaptic neuron (table 1; equation 3; Fig. 6F). The last column in Fig. 6H shows this change, taking into account the input received from all connected populations averaged over the stimulus presentation. The order of strength of the net excitatory input driving the visual response is VIP>PC>PV>SST, consistent with the effects of locomotion shown in Figs. 2 and 3. Note again that locomotion caused SSTs to receive weak net excitation during the stimulus rather than inhibition expected based on the VIP->SST->PC disinhibitory model. The overarching picture is that locomotion adjusts the gain of visual

responses by modulating both excitatory signals entering layer 2/3 and the strength of local synaptic connections[12].

Differential modulation of SST synapses onto sensitizing and depressing PCs

Why do some PCs sensitize while others depress? Optogenetic manipulations of interneurons indicate that the direction and amplitude of slow adaptation reflects the balance between PV and SST inputs[9]. PVs sensitize (Fig. 3B), so PCs in which these inputs dominate tend to depress, while SSTs depress (Fig. 3C), causing PCs in which these inputs dominate to sensitize. To make these ideas quantitative, we fit the model separately to the sensitizing, intermediate and depressing PC subpopulations (Fig. 7A-C). At rest, all the external connections to PCs had similar weights irrespective of adaptive properties; the stand-out differences were in the local inhibitory connections (Fig. 7D). In qualitative agreement with the "balance model", the direction of adaptation of a PC was dependent on the ratio of the PV and SST inputs, which increased progressively between the sensitizing, intermediate and depressing populations (1.62, 11.8 and ~84, respectively; Fig. 7D). Considered in terms of the total drive that PCs receive from each of these interneuron populations, the PV:SST input ratio was 6.2, 0.62, and 0.45 in sensitizing, intermediate and depressing PCs, respectively (Fig. 7G).

A notable feature emerges when locomotion-dependent changes in synaptic weights are calculated: while SST synapses to depressing PCs more than double in strength, the connections to the sensitizing and intermediate groups became *weaker* (Fig. 7F). SSTs are a heterogenous class of neuron and are known to target PCs in two distinct ways. The most numerous type, Martinotti cells, synapse on distal apical dendrites of PCs in layer 1 and show strong depressing adaptation similar to the population average in Fig. 3C[46,60,61]. We suggest, therefore, that Martinotti cells are the dominant type of SST connected to sensitizing PCs. In contrast, non-Martinotti cells target the soma and basal dendrites and show much weaker adaptation[59,62], suggesting that these preferentially target depressing PCs.

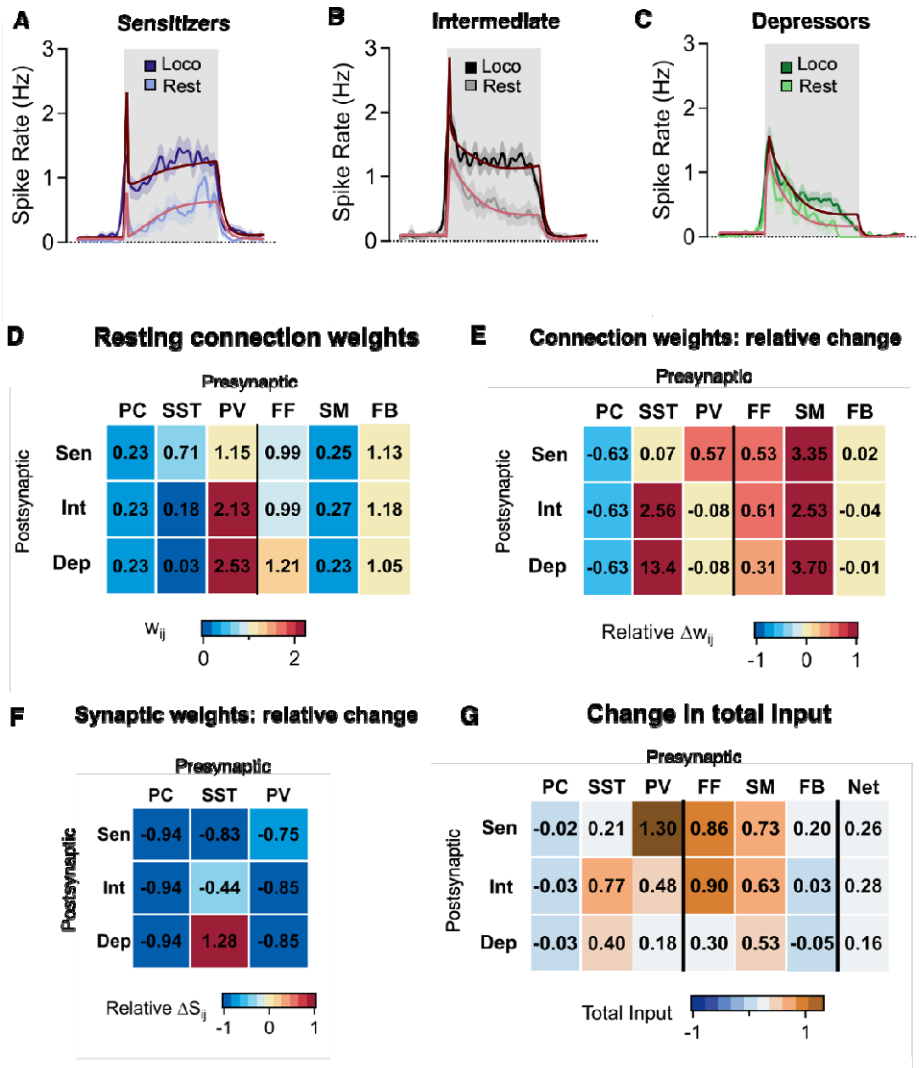

Figure 7. Differences in PV:SST input ratio determine the direction of PC adaptation and the change in gain associated with locomotion. **A.** Activity of PCs from the tertile with lower AIs (sensitizers) at rest and during locomotion together with fits calculated by the model (rest, RMSE = 0.18; loco, RMSE = 0.17). These are paired measurements from 158 neurons in 9 mice. During locomotion 7.5 ±1.2 more spikes were fired during the stimulus. **B-C.** As A, but for the intermediate and depressing tertiles. Fit RMSE varied between 0.14 and 0.19. During locomotion the stimulus generated 6.3 ± 0.9 more spikes in the intermediate group and 2.8 ± 0.4 in depressors. **D.** Heatmaps of the synaptic weights for each PC tertile at rest; sensitizers (Sen), intermediate (Int) and depressing (Dep). **E.** Relative change in connection weights caused by locomotion for each subpopulation of PCs (calculated as equation 5). The key difference is the relative strength of PV and SST inputs. **F.** Relative change in synaptic weights caused by locomotion for each subpopulation of PCs. **G.** Change in total input during presentation of the stimulus received by each subpopulation of PCs. The last column shows the *net* change in total input, taking into account the polarity of the synapse. Depressors receive less net excitation than the intermediate and sensitizing tertiles.

Discussion

Adaptation is a fundamental aspect of sensory processing across cortical areas but it has not been clear how it is adjusted by changes in behavioural state that modulate these circuits. Our results demonstrate that in layer 2/3 of mouse V1 locomotion preferentially amplifies responses in PCs that exhibit sensitizing adaptation over behavioural time-scales while exerting minimal effects on depressing PCs (Figs. 1 and 2). A combination of experiment and data-driven modelling indicates that this differential modulation of the PC population reflects two major variations in their local inhibitory circuits. First, sensitizing PCs receive proportionally stronger SST input relative to PV input (Fig. 7) making them more susceptible to the locomotion-driven increase in SST inhibitory strength (Fig. 6). Second, locomotion differentially modulates synapses of SSTs, increasing the strength of connections to depressing PCs but weakening synapses to sensitizing PCs (Fig. 7). More generally, these results build from the simple model of gain control through the VIP→SST→PC disinhibition pathway [11,63] by also considering the broader neuromodulatory actions of the cholinergic input to V1 through a model. The results indicate that locomotion increases the gain of PCs through a combination of circuit effects, including a decrease in the strength of synapses mediating feedback inhibition from PV interneurons[64] (Fig. 6 and 7).

Gating the feedforward signal

The increase in gain during locomotion was profound: the number of PCs responding to the stimulus increased by a factor of six (Table 1) and the average amplitude of those responses by a factor of 2-3 (Figs. 1 and 2). About 70–80% of PCs in layer 2/3 send axon collaterals to higher visual areas[65,66] so these combined effects will strongly amplify the feedforward visual signal, at least to the drifting grating stimulus used here. The local recurrent signals are, however, strongly damped by a wide-spread decrease in the strength of recurrent PC synapses subject to local modulation (Fig. 6). This decoupling of spiking activity and synaptic efficacy suggests a mechanism by which V1 can amplify its output to downstream targets, such as higher visual areas, without generating excessive excitation in the local recurrent network. Such a mechanism could be important for maintaining the stability of computations that rely on balanced excitation and inhibition. The suppression of PC output within V1 may therefore reflect a form of gating that allows feedforward communication to be selectively boosted while shielding local circuits from saturation. This prediction of the model is in line with the known actions of acetylcholine on presynaptic M2 receptors, which reduce glutamate release at PC terminals[16-18].

Locomotion shapes cortical dynamics through multiple pathways

The first effect of locomotion was to enhance a slow sensitizing signal activated by the visual stimulus, the major target of which was VIP interneurons (Fig. 4). The source of this signal is

likely the cholinergic input from basal forebrain [2,13-15] and optogenetic experiments demonstrate that it determined the dynamics of adaption in SST (Fig. 4 and Supplementary Figure 1). The second major effect predicted by the model was a near 90% reduction in the strength of PC synapses across all targets (Fig. 6G), consistent with a range of evidence obtained *in vitro* demonstrating that M2 muscarinic receptor-cause presynaptic inhibition[16,17,67]. A similar mechanism likely operates at PV synapses, where release probability is reduced by M2 and M4 receptors[55-57]. However, the situation is different for SST interneurons. Our modelling shows that depressing PCs receive strong SST inputs at rest and that these synapses are *potentiated* during locomotion (Fig. 7E-G). This is likely to reflect a post-synaptic action of M1 receptors which have been shown to enhance postsynaptic $GABA_A$ currents in visual and somatosensory[57,58]. In contrast, SST inputs to sensitizing PCs appeared *weaker* during locomotion (Fig. 7F).

We suggest that SSTs contacting PCs are predominantly Martinotti cells because these have been shown to depress strongly[46,60,61]. Non-Martinotti cells generate more variable responses and may dominate the input to depressing PCs, which also receive stronger inhibition from sensitizing PVs[9]. Notably, differential cholinergic modulation of Martinotti and non-Martinotti SSTs has also been observed in mouse somato-sensory cortex during whisking[59], although it may also be that other neuromodulatory systems contribute to these mixed effects, including noradrenaline, serotonin and dopamine[2,11]. The models might be refined by splitting SSTs into two separate populations once responses were measured separately in each[68] but a more important issue is to test the predicted changes in synaptic strength. The best way to do this would be to make paired electrophysological recordings of identified SST→PC connections during state transitions, but direct measurements of changes in synaptic strength in the cortex of behaving mice are very difficult - most of the available evidence is inferred from circuit-level activity patterns and *in vitro* studies.

A key insight from our modelling is that the relative strength of PV and SST inputs predicts both the direction of PC adaptation *and* the degree of locomotion-induced gain modulation (Fig. 7). Depressing PCs receive stronger PV input, consistent with the rapid and temporally precise inhibition[64]. In contrast, sensitizing PCs receive relatively stronger SST input which slowly depress to drive sensitization[9]. These differences in PV:SST ratio also contribute to the changes in gain associated with locomotion: because SST→PC weights increase substantially during locomotion (Fig. 6), PCs already dominated by SST input exhibit the largest gain enhancement. It is well established that there are substantial variations in the inhibitory input patterns to PCs but it is unclear how far these reflect the development of specific wiring patterns as opposed to the variability that will arise from random connections[35,69,70].

Modulation of SST→PC synaptic strength during changes in brain state

An intriguing prediction of our model is that SST→PC synapses onto depressing PCs strengthen selectively during locomotion (Fig. 7F). What mechanisms might underlie this effect? While direct evidence is lacking in V1, cholinergic modulation has been shown to facilitate GABA release from SST interneurons in somatosensory cortex[58,59]. In principle, this possibility might be tested by targeted recordings of identified SST→PC connections during state transitions.

Why would the cortex preferentially enhance sensitizing PCs during locomotion? One possibility is that these changes maintain responsiveness to low contrast and transient stimuli in a visual environment that has become more dynamic with a strong component of visual flow. By selectively enhancing PCs that resist rapid depression, the circuit may preserve sensitivity to behaviourally relevant stimuli[53,71]. From a computational perspective, the ability to differentially modulate adaptive subpopulations allows the cortex to tune its operating regime to changes in behaviour. These findings might also be interpreted in terms of broader theories of predictive coding and attention[72]: locomotion likely reflects an internal state of heightened predictive engagement with the environment and it may be that selective amplification of sensitizing PCs serves to enhance cortical representations of expected sensory features.

Acknowledgements

This work was supported by BBSRC grant BB/X009386/1, a PhD scholarship to SD from the Leverhulme Trust (DS-2017-011) and a Researchers at Risk Fellowship to YK from the British Academy and Council for At-Risk Academics (RaR/100503).

Methods

Animal preparation and multiphoton imaging *in vivo*

All experimental procedures in mice were conducted according to the UK Animals Scientific Procedures Act (1986). These were performed at University of Sussex under personal and project licenses granted by the Home Office following review by the Animal Welfare and Ethics Review Board.

Experiments were performed in adult mice (P90-P260) using experimental methods described in detail previously[9]. Results are reported from Results are reported from four VIP-Cre mice (VIP tm1(cre)Zjh/J Jackson #010908), fourteen SST-Cre (SST tm2.1(cre)Zjh/J, Jackson #013044), four SST-Flp (Sst tm3.1(flpo)Zjh; Jackson #028579) x VIP-Cre and ten PV-Cre (Pvalb tm1(cre)Arbr/J, Jackson #008069), from either sex. Mice were prepared for head-fixed multiphoton imaging through a surgical procedure in a stereotaxic frame under isoflurane anaesthesia. A titanium head plate was attached to the skull and a 3 mm craniotomy was drilled to expose the brain. We then expressed AAV1.CaMKII.GCaMP6f.WPRE.SV40 to image calcium activity in pyramidal cells and AAV9.CAG.Flex.GCaMP6f.WPRE.SV40 to image interneurons in Cre lines. To excite interneurons optogenetically we used rAAV9/Syn.Flex.ChrimsonR.tdTomato and to inhibit them we used AAV5.CBA.Flex.ArchT-tdToma- to.WPRE.SV40.

During imaging mice were free to run on a cylindrical treadmill placed under a two-photon microscope, with stimuli being presented on two monitors covering most of the visual field. Visual stimuli were sinusoidal gratings drifting upwards (100% contrast, 1 Hz, 10 s duration) generated using the Python library PsychoPy[73]. The standard experimental protocol consisted of ten presentations of the stimulus with a 20 s interstimulus interval. When testing optogenetic manipulations these 10 trials were interleaved with 10 additional trials paired with illumination from an amber LED. The intensity of this LED was adjusted to activity of PCs to similar levels in different experiments. Running speed was measured with a rotary encoder and recorded through the imaging software (Scanimage5; Vidrio Technologies). The two-photon microscope (Scientifica SP1) employed a 16x water immersion objective (0.8 NA; Nikon) and imaging was carried out at a depth of 150-300 μm below the surface of the brain.

Raw movies were registered and segmented into regions of interest (ROIs) using the Suite2P package running in MATLAB 2021a [74] and further analysed using custom-written code in Igor Pro 8 (Wavemetrics). Here we only analyse results from the first session in which the animal was exposed to the stimulus to avoid effects of habituation. Stimulus trials were only included for analysis if the mouse was running faster than 3 cm/s for more than 80% of the time. To calculate the response dynamics of PC, PV, SST and VIP populations we only included cells that were positively correlated with the stimulus. For each cell, the Pearson's correlation coefficients was computed between its activity trace (ΔF/F) and a stimulus trace binarized as either stimulus off

(0) or stimulus on (1) using the StatsLinearCorrelationTest Function in IgorPro (Wavemetrics). The threshold for significant positive or negative correlation was set at $p < 0.05$. Measurements of adaptive properties were confined to cells which were significantly positively correlated with the stimulus. The adaptive index (AI) was calculated from the GCaMP6f signal as AI = (R1 − R2)/(R1 + R2) where R1 is the average response over the period 0.5 - 2.5 s after stimulus onset and R2 is the average at 8-10 s.

Estimation of firing rates

To estimate firing rates from the recorded ΔF/F data we used the MLspike algorithm using initial parameters expected for GCaMP6f[23]. Briefly, this finds the optimal spike train to fit the calcium fluorescence trace (ΔF/F) taking into account estimates of baseline fluorescence level and neuronal parameters including the amplitude of the unitary Ca^{2+} transient generated by a spike (A) and the decay time-constant of that transient (τ). In general, we followed recommendations and demos in the article and on the MLspike GitHub page. We set the range for A to be between 1 and 50% and τ was set at values from 0.05 to 3 seconds. The parameter A_{max}, which corresponds to the maximum amplitude of detected events, was 9, and the saturation parameter was set to 0.002. The Hill coefficient for Ca^{2+} binding to GCaMP6f was varied in the range from 1 to 3.75 with step sizes of 0.25.

Model of the circuit in layer 2/3 of V1

We built a rate-based data-driven population model of the network circuit in the mouse visual cortex layer 2/3 (code and example data sets at https://github.com/lagnadoLab/CortexModel). The purpose of the model was to understand adaptive gain control during rest and locomoting states of four main neuron populations (PC, PV, SST, and VIP). The network was represented by the system of four mean-field first order ordinary differential equations (equation 1)[28]**.** The neuronal input-output function, $f(x)$, was a rectified power law[30]

$$f(x) = k([x]_{+}^{threshold})^{n} \qquad (6)$$

where k is a scaling coefficient which was set to 1. This is a rectified linear function with a lower threshold, $[x]_{+}^{threshold}$, of zero to prevent negative values of firing rate and upper threshold of 25 to prevent run-away behaviour of the algorithm solving the network equations system. The exponent was set to $n = 2$ but a linear activation function ($n = 1$) produced similar results during the fitting process, as observed by others[75].

Connectivity between and within populations is represented by total connection weight w_{ji} which is dependent on both the number of responsive cells in the presynaptic population and the

strength of individual synapses. The number of presynaptic neurons responding to the stimulus varied between rest and locomotion so to assess changes in synaptic strength caused by neuromodulators the total connection weight was divided by the number of responsive presynaptic cells (Table 1 and equations 2 and 4 in Results). The aim of fitting the model to the average activity traces of each neuronal population was to obtain connection weights, w_{ji}. Weights were set to zero where published work indicated that connections are very weak or non-existent, as between SST interneurons[31,36]. The final connection weights matrix for connections within layer 2/3 was represented as:

$$W = \begin{pmatrix} w_{PC_PC} & w_{PC_PV} & w_{PC_SST} & w_{PC_VIP} \\ w_{PV_PC} & w_{PV_PV} & w_{PV_SST} & w_{PV_VIP} \\ w_{SST_PC} & w_{SST_PV} & w_{SST_SST} & w_{SST_VIP} \\ w_{VIP_PC} & w_{VIP_PV} & w_{VIP_SST} & w_{VIP_VIP} \end{pmatrix} = \begin{pmatrix} w_{PC_PC} & w_{PC_PV} & w_{PC_SST} & w_{PC_VIP} \\ w_{PV_PC} & w_{PV_PV} & 0 & 0 \\ w_{SST_PC} & w_{SST_PV} & 0 & w_{SST_VIP} \\ 0 & 0 & w_{VIP_SST} & 0 \end{pmatrix} \quad (7)$$

External inputs driving activity

Three types of external input drove activity in the circuit which we termed feedforward (FF), slow modulation (SM) and feedback input (FB): the forms and origins of these are discussed in Results. These were represented in Equation 1 by the variable In that was specific for each input. The FF input was defined by the following system of equations:

$$In_{FF}(t) = \begin{cases} 0, & (t < s_{start} + s_{del}) \\ I_0 + A_f e^{-(t - s_{start} - s_{del})\lambda_f}, & (s_{start} + s_{del} + s_k > t \geq s_{start} + s_{del}) \\ I_0 + A_f e^{-(t - s_{start} - s_{del})\lambda_f} + k(t - s_{start} - s_{del}), & (s_{start} + s_{dur} \geq t \geq s_{start} + s_{del} + s_k) \\ \left(I_0 + A_f e^{-(s_{dur} - s_{del})\lambda_f} + k(s_{dur} - s_{del} - s_{start})\right) e^{-(t - s_{start} - s_{dur}) decay_f}, & (t > s_{start} + s_{dur}) \end{cases} \quad (8)$$

The initial short fast-depressing component had an amplitude A_f and decayed exponentially with a decay rate λ_f. The variables s_{start}, s_{del}, s_{dur}, s_k represent stimulus start, delay in the initiation of the response in a cell, the stimulus duration and an offset after the initial peak, respectively. This offset defined the initiation of a second slow increase in feedforward input that has been observed in response to drifting gratings lasting seconds[22,42]. At the end of the stimulus presentation, experimental traces decayed relatively slowly compared with the time-constant of the model neurons and this was accounted for by including an exponentially decaying component to the input with the argument $decay_f$.

The temporal form of the feedforward input measured experimentally reflects the application of a spatio-temporal Gabor filter to a sinusoidal wave of drifting gratings[76]. This oscillation was clear in the activity of individual PCs but less evident in population averages because neurons responded with different phases, depending on the location of their receptive fields relative to the stimulus. This 1 Hz oscillation was most clearly observed in the average

response of the SST population (Fig. 6C, bottom) which have larger receptive fields and therefore display less phase shifting[46]. We did not, therefore, attempt to model the oscillatory component of individual neuronal responses and concentrated on capturing the average activity across populations. The feedforward input (FF) was defined as a step of duration s_{dur} with initial amplitude (I_0 + A_f) which then decayed to a steady state of I_0 with time-constant 210 ms, defined by fitting the initial peak of the average PC response. The steady state was half the initial maximum with A_f = I_0. The linear increase is a simplified representation of the sensitizing behaviour observed experimentally in layer 4 activity[22,42].

The slow modulatory input was represented by the following system of equations:

$$In_{SM}(t) = \begin{cases} 0 & , (t < s_{start}) \\ \frac{A_s}{1+e^{(s_{start}+del-t)\lambda_s}} & , s_{start} + s_{dur} \geq t \geq s_{start}, \\ \frac{A_s e^{-(t-s_{start}-s_{dur})decay_s}}{1+e^{(del-s_{dur})\lambda_s}} & , (t > s_{start} + s_{dur}) \end{cases} \quad (9)$$

where s_{start}, s_{dur} represent the time of the stimulus start and the stimulus duration, respectively. The slow modulatory (SM) component is represented by a sigmoid function with an amplitude A_s, growth rate λ_s, and centre of sigmoid shifted to a del value from the stimulus starting time. Similarly to FF, the decay phase after the stimulus end was accounted for by the argument $decay_s$.

Finally, feedback input (FB) was represented by a step function:

$$In_{FB}(t) = \begin{cases} 0, & (t < s_{start} + s_{fb_{delay}}) \cup (t > s_{start} + s_{dur}) \\ A_{fb}, & \left(s_{start} + s_{dur} \geq t \geq s_{start} + s_{fb_{delay}}\right) \\ A_{fb} e^{-(t-s_{start}-s_{dur})decay_{fb}}, & (t > s_{start} + s_{dur}) \end{cases} \quad (10)$$

where s_{start}, s_{fb_delay}, s_{dur} represent time of the stimulus start, delay in the initiation of the response in a cell and the stimulus duration, respectively. The amplitude of the stimulus is defined by A_{fb}. Similarly to FF and SM, the decay phase after stimulus end was accounted for by the argument $decay_{fb}$. The amplitudes of A_{fb}, A_s and I_o were fixed around 1 Hz based on the average response of PCs during locomoting state (Fig. 2).

Fitting the model

To obtain values of connection weights we fit the model simultaneously to the average activity traces of the four neuronal populations using the *LMFIT* library in Python [77] by minimization of reduced chi-square parameter:

$$\chi^2_{reduced} = \frac{\sum_i^N (data_i - model_i)^2}{stderr_i^2 (N - N_v)}, \quad (11)$$

where $(data_i - model_i) / stderr_i$ represents the residual function weighted by uncertainties in the experimental data, N is the number of data points and N_v is the number of variable parameters. We set the threshold chi-square value to be 15. We used standard errors of the mean (S.E.M) to weight locomotion data. For the data obtained from the resting state we used S.E.M = 1. Additionally, to have a measure of fit quality independent of the data uncertainty and number of varied parameters we calculated root mean square error (RMSE) for each fit:

$$RMSE = \sqrt{\frac{\sum_i^N (data_i - model_i)^2}{N}}. \quad (12)$$

We tested several fitting methods designed for a local minimum search: *Levenberg-Marquardt, Nelder-Mead, Powell, L-BFGS-B* and noticed that *Nelder-Mead and Powell* methods worked well on the full range of values defined by minimum and maximum limits of variable parameters, while the *Levenberg-Marquardt* and *L-BFGS-B methods* were better for final precise fitting.

Different sets of parameters sometimes provided similar values of reduced chi-square in multidimensional parameter space, indicating that networks with different connectivity parameters could produce similar activity patterns[78], which in turn made the results sensitive to the initial guess of parameters. We set all weights to 0.5 as initial set of parameters for fitting. An important further constraint was provided by requiring the model to additionally fit the results of optogenetic manipulations of the PV and SST populations (Fig. 5), leading to a reduced number of sets of possible synaptic weights. In these experiments, the intensity of the LED was set to increase or decrease PV or SST activity by a known factor between 1.3 and 2, as measured empirically in other parallel experiments measuring GCaMP6f responses in these interneurons[9]. The average PV or SST activity trace was then scaled by the same factor for comparing the model to observed PC activity and RMSE value calculated for each comparison in optogenetic tests. This approach allowed us to find a stable set of parameters describing both the basic state of the circuit during locomotion and the effects of perturbing the circuit optogenetically. For fitting a resting state, we introduced initial conditions as a solution for the locomotion state and altered the initial values of

weights that are known to be dependent on locomotion: external inputs to layer 2/3 are lower at rest, as is PC excitation to all populations[12].

Fitting the model to subpopulations of pyramidal cells

The whole PC population was split into tertiles (sensitizers, intermediate cells and depressors) based on the distribution of adaptive index (Fig. 1). The average response of each subpopulation was then fit separately in the locomoting and resting states to assess changes in connectivity that describe the adaptive properties of each (Fig. 7). Three simplifying assumptions were made. First, that each subpopulation of PC receives the same shape of inputs as the average PC across the population. Second, only the synaptic weight of those connections directly targeting PCs were left free to vary while the other connections within the circuit were fixed. This was done because there is no change in activities of interneurons during separating a PC population into three subgroups and excitatory input from PCs to interneurons was taken as an average response of the whole PC population, similarly as during fitting of the whole network. Third, we used the initial conditions of the average models scaled to match amplitudes of subpopulations to average response. From Equations 1 and 6 the scaling factor is:

$$scale = \frac{w_{tertile}}{w_{avg}} = \sqrt{\frac{A_{tertile}}{A_{avg}}}, \qquad (13)$$

where w_i is a weight and A_i is an average amplitude of response during stimulus. Corresponding scaling multiplication factors for locomotion are: sensitizers = 1.1, intermediate = 1.2, depressors = 0.8, and for resting state are: sensitizers = 0.9, intermediate = 1.1, depressors = 0.9.

Statistics

For the statistical tests not directly related with the model fitting we used the analytical software Igor Pro 8 and/or SPSS ('Statistical Package for the Social Sciences', IBM). To determine if the mean of one group was significantly different from another group we used a t-test (two-sided) if the distribution was normally distributed or a non-parametric Mann–Whitney U test (MWU) if it was not. We used linear mixed modelling (LMM) to test for significant interaction between locomotion state and AI tertile (Fig. 1), because cells were not paired between locomotion and resting states. Locomotion state and AI tertile were defined as fixed variables and the animal ID was defined as the random variable. All averages are given as mean ± standard error of the mean (SEM).

Supplementary Information

Similar time-scales of sensitizing and depressing adaptation

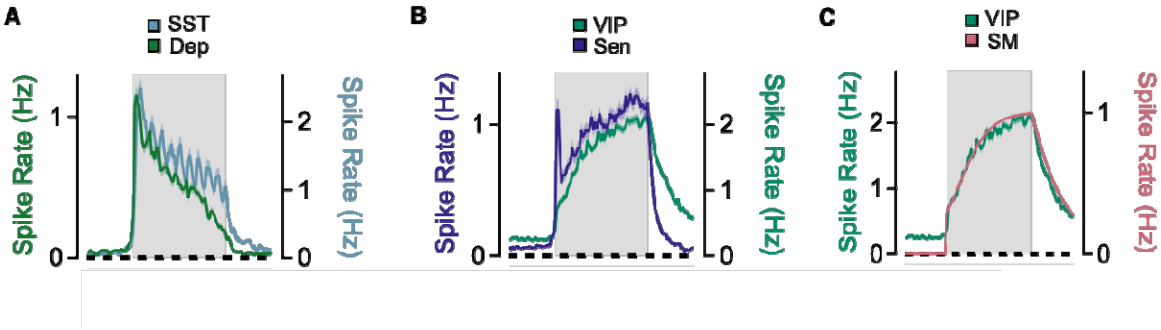

Supplementary Figure 1. Identification of an external signal determining the time-course of slow adaptation.

A. Similar dynamics of slow depression in SSTs and the depressing tertile of PCs during locomotion. **B.** Similar dynamics of sensitization in VIPs and the sensitizing tertile of PCs (left axis, blue). **C.** The slow modulatory input to the model (SM) was based on the average response of the VIP population during locomotion and consists of a step and sigmoid function with a time-constant = 1.71 s (from Fig. 4D).

References

1 Wark, B., Lundstrom, B. N. & Fairhall, A. Sensory adaptation. *Curr Opin Neurobiol* **17**, 423-429 (2007). https://doi.org/10.1016/j.conb.2007.07.001

2 Polack, P. O., Friedman, J. & Golshani, P. Cellular mechanisms of brain state-dependent gain modulation in visual cortex. *Nat Neurosci* **16**, 1331-1339 (2013). https://doi.org/10.1038/nn.3464

3 Pakan, J. M. *et al.* Behavioral-state modulation of inhibition is context-dependent and cell type specific in mouse visual cortex. *Elife* **5** (2016). https://doi.org/10.7554/eLife.14985

4 McGinley, M. J., David, S. V. & McCormick, D. A. Cortical Membrane Potential Signature of Optimal States for Sensory Signal Detection. *Neuron* **87**, 179-192 (2015). https://doi.org/10.1016/j.neuron.2015.05.038

5 Lin, P. A., Asinof, S. K., Edwards, N. J. & Isaacson, J. S. Arousal regulates frequency tuning in primary auditory cortex. *Proc Natl Acad Sci U S A* **116**, 25304-25310 (2019). https://doi.org/10.1073/pnas.1911383116

6 Adesnik, H. Synaptic Mechanisms of Feature Coding in the Visual Cortex of Awake Mice. *Neuron* **95**, 1147-1159 e1144 (2017). https://doi.org/10.1016/j.neuron.2017.08.014

7 Varela, J. A. *et al.* A Quantitative Description of Short-Term Plasticity at Excitatory Synapses in Layer 2/3 of Rat Primary Visual Cortex. *The Journal of Neuroscience* **17**, 7926-7940 (1997). https://doi.org/10.1523/JNEUROSCI.17-20-07926.1997

8 Chance, F. S., Nelson, S. B. & Abbott, L. F. Synaptic Depression and the Temporal Response Characteristics of V1 Cells. *The Journal of Neuroscience* **18**, 4785-4799 (1998). https://doi.org/10.1523/JNEUROSCI.18-12-04785.1998

9 Heintz, T. G., Hinojosa, A. J., Dominiak, S. E. & Lagnado, L. Opposite forms of adaptation in mouse visual cortex are controlled by distinct inhibitory microcircuits. *Nature Communications* **13**, 1031 (2022). https://doi.org/10.1038/s41467-022-28635-8

10 Niell, C. M. & Stryker, M. P. Modulation of visual responses by behavioral state in mouse visual cortex. *Neuron* **65**, 472-479 (2010). https://doi.org/10.1016/j.neuron.2010.01.033

11 Fu, Y. *et al.* A cortical circuit for gain control by behavioral state. *Cell* **156**, 1139-1152 (2014). https://doi.org/10.1016/j.cell.2014.01.050

12 Dipoppa, M. *et al.* Vision and Locomotion Shape the Interactions between Neuron Types in Mouse Visual Cortex. *Neuron* **98**, 602-615.e608 (2018). https://doi.org/10.1016/j.neuron.2018.03.037

13 Goard, M. & Dan, Y. Basal forebrain activation enhances cortical coding of natural scenes. *Nat Neurosci* **12**, 1444-1449 (2009). https://doi.org/10.1038/nn.2402

14 Pronneke, A. *et al.* Characterizing VIP Neurons in the Barrel Cortex of VIPcre/tdTomato Mice Reveals Layer-Specific Differences. *Cereb Cortex* **25**, 4854-4868 (2015). https://doi.org/10.1093/cercor/bhv202

15 Lohani, S. *et al.* Spatiotemporally heterogeneous coordination of cholinergic and neocortical activity. *Nat Neurosci* **25**, 1706-1713 (2022). https://doi.org/10.1038/s41593-022-01202-6

16 Kimura, F. & Baughman, R. W. Distinct muscarinic receptor subtypes suppress excitatory and inhibitory synaptic responses in cortical neurons. *J Neurophysiol* **77**, 709-716 (1997). https://doi.org/10.1152/jn.1997.77.2.709

17 Hasselmo, M. E. & Bower, J. M. Cholinergic suppression specific to intrinsic not afferent fiber synapses in rat piriform (olfactory) cortex. *J Neurophysiol* **67**, 1222-1229 (1992). https://doi.org/10.1152/jn.1992.67.5.1222

18 Mrzljak, L., Levey, A. I. & Goldman-Rakic, P. S. Association of m1 and m2 muscarinic receptor proteins with asymmetric synapses in the primate cerebral cortex: morphological evidence for cholinergic modulation of excitatory neurotransmission. *Proc Natl Acad Sci U S A* **90**, 5194-5198 (1993). https://doi.org/10.1073/pnas.90.11.5194

19 Haider, B., Hausser, M. & Carandini, M. Inhibition dominates sensory responses in the awake cortex. *Nature* **493**, 97-100 (2013). https://doi.org/10.1038/nature11665

20 Jouhanneau, J. S., Kremkow, J., Dorrn, A. L. & Poulet, J. F. In Vivo Monosynaptic Excitatory Transmission between Layer 2 Cortical Pyramidal Neurons. *Cell Rep* **13**, 2098-2106 (2015). https://doi.org/10.1016/j.celrep.2015.11.011

21 Pala, A. & Petersen, C. C. H. In vivo measurement of cell-type-specific synaptic connectivity and synaptic transmission in layer 2/3 mouse barrel cortex. *Neuron* **85**, 68-75 (2015). https://doi.org/10.1016/j.neuron.2014.11.025

22 Keller, A. J. *et al.* A Disinhibitory Circuit for Contextual Modulation in Primary Visual Cortex. *Neuron* **108**, 1181-1193.e1188 (2020). https://doi.org/10.1016/j.neuron.2020.11.013

23 Deneux, T. *et al.* Accurate spike estimation from noisy calcium signals for ultrafast three-dimensional imaging of large neuronal populations in vivo. *Nature Communications* **7**, 12190 (2016). https://doi.org/10.1038/ncomms12190

24 Friedrich, J., Zhou, P. & Paninski, L. Fast online deconvolution of calcium imaging data. *PLoS Comput Biol* **13**, e1005423 (2017). https://doi.org/10.1371/journal.pcbi.1005423

25 Rupprecht, P. *et al.* A database and deep learning toolbox for noise-optimized, generalized spike inference from calcium imaging. *Nat Neurosci* **24**, 1324-1337 (2021). https://doi.org/10.1038/s41593-021-00895-5

26 Berens, P. *et al.* Community-based benchmarking improves spike rate inference from two-photon calcium imaging data. *PLoS computational biology* **14**, e1006157 (2018).

27 Fairhall, A. L., Lewen, G. D., Bialek, W. & de Ruyter Van Steveninck, R. R. Efficiency and ambiguity in an adaptive neural code. *Nature* **412**, 787-792 (2001). https://doi.org/10.1038/35090500

28 Wilson, H. R. & Cowan, J. D. Excitatory and Inhibitory Interactions in Localized Populations of Model Neurons. *Biophysical Journal* **12**, 1-24 (1972). https://doi.org/10.1016/S0006-3495(72)86068-5

29 Miller, K. D. & Troyer, T. W. Neural Noise Can Explain Expansive, Power-Law Nonlinearities in Neural Response Functions. *Journal of Neurophysiology* **87**, 653-659 (2002). https://doi.org/10.1152/jn.00425.2001

30 Rubin, Daniel B., Van Hooser, Stephen D. & Miller, Kenneth D. The Stabilized Supralinear Network: A Unifying Circuit Motif Underlying Multi-Input Integration in Sensory Cortex. *Neuron* **85**, 402-417 (2015). https://doi.org/10.1016/j.neuron.2014.12.026

31 Pfeffer, C. K., Xue, M., He, M., Huang, Z. J. & Scanziani, M. Inhibition of inhibition in visual cortex: the logic of connections between molecularly distinct interneurons. *Nature Neuroscience* **16**, 1068-1076 (2013). https://doi.org/10.1038/nn.3446

32 Karnani, M. M. *et al.* Cooperative Subnetworks of Molecularly Similar Interneurons in Mouse Neocortex. *Neuron* **90**, 86-100 (2016). https://doi.org/10.1016/j.neuron.2016.02.037

33 Brunel, N. Dynamics of sparsely connected networks of excitatory and inhibitory spiking neurons. *J Comput Neurosci* **8**, 183-208 (2000). https://doi.org/10.1023/a:1008925309027

34 Deco, G., Jirsa, V. K., Robinson, P. A., Breakspear, M. & Friston, K. The dynamic brain: from spiking neurons to neural masses and cortical fields. *PLoS Comput Biol* **4**, e1000092 (2008). https://doi.org/10.1371/journal.pcbi.1000092

35 Jiang, X. L. *et al.* Principles of connectivity among morphologically defined cell types in adult neocortex. *Science* **350** (2015). https://doi.org/ARTN aac9462

10.1126/science.aac9462

36 Hage, T. A. *et al.* Synaptic connectivity to L2/3 of primary visual cortex measured by two-photon optogenetic stimulation. *eLife* **11**, e71103 (2022). https://doi.org/10.7554/eLife.71103

37 Campagnola, L. *et al.* Local connectivity and synaptic dynamics in mouse and human neocortex. *Science* **375**, eabj5861 (2022). https://doi.org/10.1126/science.abj5861

38 Oh, S. W. *et al.* A mesoscale connectome of the mouse brain. *Nature* **508**, 207-214 (2014). https://doi.org/10.1038/nature13186

39 Froudarakis, E. *et al.* The Visual Cortex in Context. *Annu Rev Vis Sci* **5**, 317-339 (2019). https://doi.org/10.1146/annurev-vision-091517-034407

40 Roelfsema, P. R., Lamme, V. A. & Spekreijse, H. Object-based attention in the primary visual cortex of the macaque monkey. *Nature* **395**, 376-381 (1998). https://doi.org/10.1038/26475

41 Leinweber, M., Ward, D. R., Sobczak, J. M., Attinger, A. & Keller, G. B. A Sensorimotor Circuit in Mouse Cortex for Visual Flow Predictions. *Neuron* **96**, 1204 (2017). https://doi.org/10.1016/j.neuron.2017.11.009

42 Makino, H. & Komiyama, T. Learning enhances the relative impact of top-down processing in the visual cortex. *Nature Neuroscience* **18**, 1116-1122 (2015). https://doi.org/10.1038/nn.4061

43 Fiser, A. *et al.* Experience-dependent spatial expectations in mouse visual cortex. *Nat Neurosci* **19**, 1658-1664 (2016). https://doi.org/10.1038/nn.4385

44 Zhang, S. *et al.* Long-range and local circuits for top-down modulation of visual cortex processing. *Science* **345**, 660-665 (2014). https://doi.org/doi:10.1126/science.1254126

45 Jin, M. & Glickfeld, L. L. Mouse Higher Visual Areas Provide Both Distributed and Specialized Contributions to Visually Guided Behaviors. *Curr Biol* **30**, 4682-4692.e4687 (2020). https://doi.org/10.1016/j.cub.2020.09.015

46 Adesnik, H., Bruns, W., Taniguchi, H., Huang, Z. J. & Scanziani, M. A neural circuit for spatial summation in visual cortex. *Nature* **490**, 226-231 (2012). https://doi.org/10.1038/nature11526

47 Keller, G. B. & Mrsic-Flogel, T. D. Predictive Processing: A Canonical Cortical Computation. *Neuron* **100**, 424-435 (2018). https://doi.org/https://doi.org/10.1016/j.neuron.2018.10.003

48 Yogesh, B. & Keller, G. B. Cholinergic input to mouse visual cortex signals a movement state and acutely enhances layer 5 responsiveness. *Elife* **12** (2024). https://doi.org/10.7554/eLife.89986

49 Shen, S. *et al.* Distinct organization of two cortico-cortical feedback pathways. *Nat Commun* **13**, 6389 (2022). https://doi.org/10.1038/s41467-022-33883-9

50 Liu, Y. *et al.* Organization of corticocortical and thalamocortical top-down inputs in the primary visual cortex. *Nat Commun* **15**, 4495 (2024). https://doi.org/10.1038/s41467-024-48924-8

51 Jordan, R. & Keller, G. B. Opposing Influence of Top-down and Bottom-up Input on Excitatory Layer 2/3 Neurons in Mouse Primary Visual Cortex. *Neuron* **108**, 1194-1206.e1195 (2020). https://doi.org/10.1016/j.neuron.2020.09.024

52 Kim, E. J., Jacobs, M. W., Ito-Cole, T. & Callaway, E. M. Improved Monosynaptic Neural Circuit Tracing Using Engineered Rabies Virus Glycoproteins. *Cell Rep* **15**, 692-699 (2016). https://doi.org/10.1016/j.celrep.2016.03.067

53 Dadarlat, M. C. & Stryker, M. P. Locomotion Enhances Neural Encoding of Visual Stimuli in Mouse V1. *J Neurosci* **37**, 3764-3775 (2017). https://doi.org/10.1523/JNEUROSCI.2728-16.2017

54 Erisken, S. *et al.* Effects of Locomotion Extend throughout the Mouse Early Visual System. *Current Biology* **24**, 2899-2907 (2014). https://doi.org/10.1016/j.cub.2014.10.045

55 Xiang, Z., Huguenard, J. R. & Prince, D. A. GABAA receptor-mediated currents in interneurons and pyramidal cells of rat visual cortex. *J Physiol* **506 (Pt 3)**, 715-730 (1998). https://doi.org/10.1111/j.1469-7793.1998.715bv.x

56 Kruglikov, I. & Rudy, B. Perisomatic GABA release and thalamocortical integration onto neocortical excitatory cells are regulated by neuromodulators. *Neuron* **58**, 911-924 (2008). https://doi.org/10.1016/j.neuron.2008.04.024

57 Urban-Ciecko, J. & Barth, A. L. Somatostatin-expressing neurons in cortical networks. *Nat Rev Neurosci* **17**, 401-409 (2016). https://doi.org/10.1038/nrn.2016.53

58 Chen, N., Sugihara, H. & Sur, M. An acetylcholine-activated microcircuit drives temporal dynamics of cortical activity. *Nat Neurosci* **18**, 892-902 (2015). https://doi.org/10.1038/nn.4002

59 Muñoz, W., Tremblay, R., Levenstein, D. & Rudy, B. Layer-specific modulation of neocortical dendritic inhibition during active wakefulness. *Science* **355**, 954-959 (2017).

60 Wang, Y., Gupta, A., Toledo-Rodriguez, M., Wu, C. Z. & Markram, H. Anatomical, physiological, molecular and circuit properties of nest basket cells in the developing somatosensory cortex. *Cereb Cortex* **12**, 395-410 (2002). https://doi.org/10.1093/cercor/12.4.395

61 Silberberg, G. & Markram, H. Disynaptic inhibition between neocortical pyramidal cells mediated by Martinotti cells. *Neuron* **53**, 735-746 (2007). https://doi.org/10.1016/j.neuron.2007.02.012

62 Tasic, B. *et al.* Shared and distinct transcriptomic cell types across neocortical areas. *Nature* **563**, 72-78 (2018).

63 Pi, H.-J. *et al.* Cortical interneurons that specialize in disinhibitory control. *Nature* **503**, 521-524 (2013). https://doi.org/10.1038/nature12676

64 Atallah, B. V., Bruns, W., Carandini, M. & Scanziani, M. Parvalbumin-expressing interneurons linearly transform cortical responses to visual stimuli. *Neuron* **73**, 159-170 (2012). https://doi.org/10.1016/j.neuron.2011.12.013

65 Glickfeld, L. L., Andermann, M. L., Bonin, V. & Reid, R. C. Cortico-cortical projections in mouse visual cortex are functionally target specific. *Nat Neurosci* **16**, 219-226 (2013). https://doi.org/10.1038/nn.3300

66 Han, Y. *et al.* The logic of single-cell projections from visual cortex. *Nature* **556**, 51-56 (2018). https://doi.org/10.1038/nature26159

67 Gil, Z., Connors, B. W. & Amitai, Y. Differential regulation of neocortical synapses by neuromodulators and activity. *Neuron* **19**, 679-686 (1997). https://doi.org/10.1016/s0896-6273(00)80380-3

68 Tremblay, R., Lee, S. & Rudy, B. GABAergic Interneurons in the Neocortex: From Cellular Properties to Circuits. *Neuron* **91**, 260-292 (2016). https://doi.org/10.1016/j.neuron.2016.06.033

69 Fino, E. & Yuste, R. Dense Inhibitory Connectivity in Neocortex. *Neuron* **69**, 1188-1203 (2011). https://doi.org/https://doi.org/10.1016/j.neuron.2011.02.025

70 Hofer, S. B. *et al.* Differential connectivity and response dynamics of excitatory and inhibitory neurons in visual cortex. *Nature neuroscience* **14**, 1045-1052 (2011).

71 Bennett, C., Arroyo, S. & Hestrin, S. Subthreshold mechanisms underlying state-dependent modulation of visual responses. *Neuron* **80**, 350-357 (2013). https://doi.org/10.1016/j.neuron.2013.08.007

72 Rao, R. P. & Ballard, D. H. Predictive coding in the visual cortex: a functional interpretation of some extra-classical receptive-field effects. *Nat Neurosci* **2**, 79-87 (1999). https://doi.org/10.1038/4580

73 Peirce, J. W. PsychoPy--Psychophysics software in Python. *J Neurosci Methods* **162**, 8-13 (2007). https://doi.org/10.1016/j.jneumeth.2006.11.017

74 Pachitariu, M. *et al.* in *bioRxiv* 061507 (2016).

75 Kuchibhotla, K. V. *et al.* Parallel processing by cortical inhibition enables context-dependent behavior. *Nature Neuroscience* **20**, 62-71 (2017). https://doi.org/10.1038/nn.4436

76 Gáspár, M. E., Polack, P.-O., Golshani, P., Lengyel, M. & Orbán, G. Representational untangling by the firing rate nonlinearity in V1 simple cells. *eLife* **8**, e43625 (2019). https://doi.org/10.7554/eLife.43625

77 LMFIT: Non-Linear Least-Square Minimization and Curve-Fitting for Python (Zenodo, 2014).

78 Prinz, A. A., Bucher, D. & Marder, E. Similar network activity from disparate circuit parameters. *Nat Neurosci* **7**, 1345-1352 (2004). https://doi.org/10.1038/nn1352